MAY 30 1991

NAS1.15:4225

NASA Technical Memorandum 4225

Thermomechanical and Bithermal Fatigue Behavior of Cast B1900 + Hf and Wrought Haynes 188

Gary R. Halford, Michael J. Verrilli, Sreeramesh Kalluri,
Frank J. Ritzert, Rob E. Duckert, and Frederic A. Holland

APRIL 1991

NASA

NASA Technical Memorandum 4225

Thermomechanical and Bithermal Fatigue Behavior of Cast B1900 + Hf and Wrought Haynes 188

Gary R. Halford and Michael J. Verrilli
Lewis Research Center
Cleveland, Ohio

Sreeramesh Kalluri
Sverdrup Technology, Inc.
Lewis Research Center Group
Brook Park, Ohio

Frank J. Ritzert
Lewis Research Center
Cleveland, Ohio

Rob E. Duckert
University of Wisconsin
Madison, Wisconsin

Frederic A. Holland
Lewis Research Center
Cleveland, Ohio

National Aeronautics and Space Administration
Office of Management
Scientific and Technical Information Division

1991

I

Summary

High-temperature thermomechanical and bithermal fatigue behavior was investigated for two superalloys: cast nickel-base B1900+Hf and wrought cobalt-base Haynes 188. Experimental results were generated to support development of an advanced thermal fatigue life prediction method. Strain-controlled thermomechanical and load-controlled, strain-limited, bithermal fatigue tests were used to determine the fatigue crack initiation and cyclic stress-strain response characteristics of the superalloys. Bithermal temperatures of 483 and 871 °C were used for B1900+Hf, and 316 and 760 °C for Haynes 188. Thermomechanical fatigue tests were conducted by using maximum and minimum temperatures corresponding to those for the bithermal experiments. Lives cover the range from about 10 to 3000 cycles to failure. Isothermal fatigue results obtained previously are also discussed.

Introduction

Fatigue and thermal fatigue cracking failures of structural components in high-performance equipment are common problems facing the aerospace propulsion industry. These failures are costly because they limit the usable lifetimes of expensive equipment. Yearly costs are on the order of hundreds of millions of dollars (ref. 1). These circumstances have led to intensive research (ref. 2) to better understand, describe, and predict thermal fatigue resistance of structural components and materials. This report presents the experimental results of one such research study into the thermal fatigue resistance of two high-temperature aerospace structural alloys: cast B1900+Hf and Haynes 188. A companion paper (ref. 3) deals with engineering life prediction aspects.

The term "thermomechanical fatigue" (TMF) is used to describe a laboratory testing condition that is a simplified simulation of the thermal fatigue process that occurs in structural components. In such components, temperature gradients within the solid produce differential thermal expansions which, in turn, impose local mechanical strains. These mechanical strains are known to be very important in governing thermal fatigue lifetimes, but they cannot be measured directly. Rather, they must be determined through computations using principles of solid mechanics. The magnitudes of the thermally induced mechanical strains are inextricably coupled with the magnitudes and time rates of change of temperature and the geometry of the solid (as well as thermal properties such as thermal conductivity and surface heat transfer coefficients). This situation renders thermal fatigue testing ineffective as a research tool for studying the independent effects of temperature, time, and strainrange. Thermomechanical fatigue has been introduced in recent years as a means of studying the effects of these important variables on a material's thermal cycling resistance. In a typical TMF test, the primary variables of temperature and mechanical strainrange and the time rate of change of these variables, and their respective phasings, can be measured directly and controlled independently of one another. In TMF testing, spatial thermal gradients are intentionally reduced to near zero, thus negating the requirement for solid mechanics analyses in order to ascertain the values of the important variables. TMF tests such as those discussed here will enable the development and evaluation of a method for predicting the thermal fatigue resistance of high-temperature aerospace structural alloys.

The experimental results presented were obtained to evaluate a recently proposed thermomechanical fatigue (TMF) life prediction method (ref. 4). The method, referred to as TMF/TS–SRP, is based on three recent innovations: (1) the total strain version of strainrange partitioning (TS–SRP) (ref. 5), (2) unified cyclic constitutive modeling, and (3) bithermal fatigue (BTF) testing. The method requires, as input, two types of experimental information: flow and failure behavior of the material of interest.

Flow behavior refers to the cyclic stress-strain-temperature-time response characteristics that permit the evaluation of the constants in unified viscoplastic constitutive models or in sets of less sophisticated empirical equations that accomplish the same purpose. Flow behavior is determined from the results of cyclic stress-strain tests performed over a range of strainranges, strain rates, hold times, waveshapes, and temperatures. Although failure tests are too expensive to be conducted at low strainranges and long times per cycle, flow tests can be conducted in this difficult regime if cyclic stability is achieved long before failure processes set in. Such flow tests can be used to improve the accuracy of predicting cyclic lives of low-strainrange, long-time-to-failure TMF tests or thermal fatigue lives of long-lived structural components. Some short-time-to-failure flow information is provided by the bithermal cycling tests used to document the failure behavior.

Failure behavior refers to the inelastic-strainrange-versus-cyclic-crack-initiation life relation as recognized, for example,

by the method of Strainrange Partitioning (SRP). Failure behavior for the TMF/TS-SRP approach (ref. 3) can be determined from inphase and out-of-phase BTF and bithermal creep-fatigue (BTC-F) tests. These tests are designed to capture the first-order effects of the interaction of creep, fatigue, and environmental degradation under idealized thermal cycling conditions. Bithermal experiments have been conducted and their results are presented in this report. In addition, several triangular-waveshape inphase and out-of-phase thermomechanical experiments were also conducted to create a data base for verifying the accuracy of the TMF/TS-SRP life prediction method (ref. 3).

Symbols

B	coefficient of elastic strainrange versus life relation
B'	coefficient of elastic strainrange versus life relation for forced exponent $b = -0.13$
C	coefficient of inelastic strainrange versus life relation
C'	coefficient of inelastic strainrange versus life relation for forced exponent $c = -0.70$
E	modulus of elasticity
K	cyclic strain-hardening coefficient (elastic versus inelastic strainranges)
K'	cyclic strain-hardening coefficient for a forced cyclic strain hardening exponent $n = 0.186$
N	number of applied cycles
t	time
Δ	range of variable
ϵ	axial strain
ϵ^D	diametral strain
μ	Poisson's ratio
σ	axial stress

Superscripts

b	exponent on cyclic life for elastic strainrange versus life relation
c	exponent on cyclic life for inelastic strainrange versus life relation
n	cyclic strain-hardening exponent

Subscripts

comp	compression
el	elastic
f	failure
in	inelastic
tens	tension
t	total

Experimental Details

Materials

B1900+Hf is a cast $\gamma - \gamma'$ nickel-base superalloy used in gas turbine engines for high-pressure turbine blade and inlet guide vane applications. It has excellent high-temperature strength and oxidation resistance. The material used in this study was procured by Pratt & Whitney Aircraft (PWA) under contract to NASA (ref. 6). Heat treatment, characteristics of the microstructure, chemical composition, tensile and creep properties, and isothermal fatigue resistance of the alloy are documented in references 6 to 9.

Haynes 188 is a wrought cobalt-base superalloy with both aeronautical and aerospace applications. It has been used for gas turbine combustor liners and for tubes carrying high-pressure cryogenic oxygen through zones of steam-rich, high-pressure, high-temperature hydrogen in the space shuttle main engine. This alloy has high strength and ductility at elevated temperatures. In addition, it exhibits good environmental resistance to oxidation at high temperatures and hydrogen embrittlement at low temperatures. The chemical composition, hardness, and isothermal fatigue characteristics of this alloy have been documented previously (ref. 10). Typical handbook tensile properties are reported in reference 9.

Specimens and Equipment

Hourglass-shaped fatigue specimens (ref. 10) were used for both alloys. All specimens were tested in the bare (i.e., uncoated) condition. All fatigue experiments were conducted in uniaxial, servohydraulic testing machines under computer control. The specimens were heated in an ambient laboratory environment with an alternating-current, direct-resistance heating technique. Strains were measured with a diametral extensometer positioned at the minimum cross section of the hourglass specimen. Axial strainrange values were calculated from stress-versus-diametral-strain hysteresis loop information as indicated in the appendix. Temperature measurements and control were accomplished with an optical pyrometer for the B1900+Hf. In the case of Haynes 188, Chromel-Alumel thermocouples were spot-welded at a calibrated distance from the minimum cross section.

Experimental Procedures and Test Conditions

Isothermal fatigue.—Isothermal fatigue experiments consisted of high-rate, continuous strain-cycling (HRSC) fatigue testing, which was conducted at a high enough frequency to preclude detectable creep deformation. Since the inelastic strainrange is considered to be composed of plasticity (P) in both tension and compression, this testing is designated as HRSC (PP). In the present case, a frequency of 0.2 Hz was used for B1900+Hf and frequencies of 0.2 Hz or higher for Haynes 188. A schematic hysteresis loop for an HRSC cycle is shown in figure 1(a). Both sinusoidal and triangular strain-versus-time waveforms were used.

Bitherma! fatigue and creep-fatigue.—Bithermal fatigue and creep-fatigue experiments (ref. 11) were of four test types:

(1) Bithermal, high-rate, inphase, continuous strain cycle producing 100 percent PP strainrange (HRIP (PP))
(2) Bithermal, high-rate, out-of-phase, continuous strain cycle producing 100 percent PP strainrange (HROP (PP))
(3) Bithermal, tensile creep, inphase, compressive plasticity cycle producing CP and PP strainranges (TCIP (CP + PP))
(4) Bithermal, compressive creep, out-of-phase, tensile plasticity cycle producing PC and PP strainranges (CCOP (PC + PP))

The term "creep-fatigue" is used since the cycles strongly emphasize creep deformation superimposed on strain-limited fatigue cycling. Since the tests were performed on bare specimens in a laboratory air atmosphere, they were also subjected to environmental attack in the form of oxidation. Without resorting to vacuum or inert gas environments, or to test cycles that specifically exclude creep deformation, it is difficult, at the macroscopic, phenomenological level, to partition the damage due to individual actions of fatigue, creep, and environmental attack. Even if such discriminating experiments were to be conducted, there remains the issue of dealing with complex synergistic interactions that likely accompany the presence of all three. Thus, for our present purposes, it is understood that the "creep-fatigue" experiments produced results that reflect the interactions of all three important factors: fatigue, creep, and oxidation.

HRIP (PP) and HROP (PP) are high-rate strain cycling tests similar to HRSC (PP) except that at each zero load crossing point, the load is held at zero (thus precluding application of external mechanical strain during this crucial time period when the temperature is changed) while the isothermal temperature of the specimen is changed from the maximum to the minimum, or vice versa. Once the temperature has stabilized at the current level, high-rate straining is resumed until the strain limit is reached, the strain direction reversed, and unloading occurs until zero load is again reached. For HRIP tests, the tensile plastic deformation (P) is applied at the maximum temperature while the compressive plastic deformation is imposed at the minimum temperature. The HROP designation refers to the opposite phasing of temperature and deformation. Schematic hysteresis loops of the two bithermal PP types are shown in figures 1(b) and (c). Displacement of the tensile and compressive halves of the hysteresis loops along the strain axes at zero load is due to the thermal expansion and contraction of the specimen during heating and cooling.

For the TCIP (CP + PP) tests, as with the HRIP and HROP tests, the temperature is changed from the maximum to the minimum, and vice versa, at each zero load crossing. During the tensile stress half of the cycle, the temperature is held constant at the maximum prescribed value, and an applied load is also held constant. Tensile creep deformation (C) occurs with time until the prescribed total tensile strain limit has been reached. Then, the load is decreased to zero and held at zero while the temperature is decreased to the selected minimum value. Immediately upon temperature stabilization, the specimen is loaded at a high rate (plasticity, P) into compression until the equal and opposite compressive strain limit is reached. At that point, the direction of straining is reversed and the load is dropped rapidly to zero. Under zero load control, the temperature is increased to the maximum, whereupon, following temperature stabilization, the tensile creep load again is applied rapidly and held constant. The procedure repeats until failure of the laboratory specimen occurs. The criterion for failure of the specimen is defined later in this report. A TCIP hysteresis loop is shown schematically in figure 1(d).

The CCOP (PC + PP) test is conducted in essentially the same manner as a TCIP (CP) test with the exception that the roles of tension and compression are reversed, giving rise to compressive creep (C) at the high temperature and tensile plasticity (P) at the low temperature. Figure 1(e) illustrates a typical CCOP hysteresis loop.

Data from bithermal experiments and companion flow experiments are used to determine the constants in the TMF/TS-SRP life prediction method (ref. 3).

Thermomechanical fatigue.—Thermomechanical fatigue tests were performed as verification experiments for the TMF/TS-SRP life prediction method. Both inphase and out-of-phase TMF tests were performed.

The inphase experiments, designated TMIP (CP + PP), were performed under constant strain rate control. The strain versus time history is a triangular waveshape. Similarly, the temperature is varied linearly with time in a triangular waveshape corresponding to exactly the same frequency as the cyclic straining, and with a 0° phase angle between temperature and strain (defined as peak tensile strain occurring simultaneously with the maximum temperature). These are referred to as in-phase TMF cycles. A typical TMIP hysteresis loop is shown schematically in figure 1(f).

The TMOP (PC + PP) experiments were identical to the TMIP experiments with the exception that the temperature and strain phase angle was 180° (peak tensile strain occurring simultaneously with the minimum temperature). These are referred to as out-of-phase TMF cycles. Figure 1(g) illustrates a schematic TMOP hysteresis loop.

The maximum and minimum temperatures selected for both the bithermal and the thermomechanical experiments were 871 and 483 °C for B1900+Hf and 760 and 316 °C for Haynes 188. These temperatures were selected from the following criteria. The maximum temperature was dictated by two primary concerns: (1) expected maximum service temperature, and (2) a high temperature corresponding to deformation mechanisms distinct from those at the low temperature selected. In the present cases, the maximum temperatures were taken near the ductility minimum temperatures, as shown in figure 2. Here, percent elongation, as reported in reference 9, was used as the measure of ductility. Percent reduction of area is preferable; however, sources of reliable reduction of area data were unavailable for either alloy. The minimum temper-

ature was dictated by three concerns: (1) to cover as broad and realistic a range of temperature as possible, commensurate with the anticipated usage, (2) to ensure that the minimum temperature is low enough to capture deformation mechanisms that would be operative in the application, and (3) to keep the minimum temperature high enough to avoid lengthy test times per cycle (due to long cool-down times brought about by relatively slow natural cooling of the specimen).

Before starting either a bithermal or a thermomechanical test, the temperature of the specimen was cycled several times between the maximum and minimum while it was under zero load control. This achieved thermal stability of the system as well as permitted exact measurement of the magnitude of the thermal component of the diametral strain history. The total diametral strain limits for both types of testing were calculated by adding the measured thermal strains to the previously selected mechanical diametral strains.

The temperature, load, and strain data acquisition for the B1900+Hf tests was accomplished with a computerized system (ref. 12). In the Haynes 188 program, these data were monitored continuously throughout each test on analog strip chart recorders, and the hysteresis loops were periodically recorded on an analog x-y recorder. Both flow and failure tests of the bithermal type were conducted with B1900+Hf and Haynes 188. Only failure tests were conducted under thermomechanical conditions (i.e., TMIP or TMOP). Out-of-phase bithermal and thermomechanical tests were performed on both alloys. Inphase bithermal and thermomechanical tests were performed only for the Haynes 188. Few tests were performed on the Haynes 188 alloy because of a limited quantity of material. For the cyclic failure tests, the number of cycles to failure (i.e., the macrocrack initiation life) was taken as the number of cycles at which the peak tensile load response dropped to only 50 percent of its steady-state value (usually near the half-life of the specimen). Occasionally, the specimen would separate into two pieces before reaching a 50-percent tensile load drop. Specimen separation was then used to define the number of cycles to failure. Table I summarizes the test conditions of the various types of failure tests performed on each alloy.

Although not reported here, additional flow tests of the bithermal type were conducted to determine cyclic inelastic constitutive (stress-strain temperature versus time) response characteristics for strainranges at and below those of the failure tests. These results were obtained to impart greater confidence in the numerical values of the constants in the empirical flow relations. These in turn would be expected to increase the accuracy of extrapolations required for life predictions made in the low-strain, long-life regime. A different specimen was used for each flow test waveform (i.e., inphase, out-of-phase, PP, PC, CP, etc.) of loading. Before documenting stress-strain data for use, each specimen was cycled at selected strainranges until the hysteresis loop appeared to have stabilized. Stabilization occurred within 10 to 50 cycles depending on strainrange. High strainrange tests stabilized in fewer cycles than low strainrange tests. Flow tests were conducted by starting with the smallest strainrange and working toward progressively larger values. In this way, there was a minimal effect of prior cycling on the cyclic stress-strain response as well as on the accumulation of fatigue damage which, under the circumstances, would be nonlinear and would result in lower rates of damage accumulation than if the cycle ordering were reversed (ref. 13).

Results

B1900+Hf Flow and Failure Behavior

Tensile tests.—Tensile test results for this material are reported in references 6 to 8. Averaged values of elastic modulus and strength are reproduced in table II together with typical handbook values of tensile elongation (ref. 9).

Isothermal and bithermal fatigue.—HRSC (PP) isothermal fatigue tests were performed at the maximum (871 °C) and minimum (483 °C) temperatures of the bithermal and thermomechanical tests. These results are listed in table III. The only high-strain rate, BTF data generated were from three out-of-phase, HROP (PP) tests (table III(b)). In this report all strains are mechanical strains. Figure 3 shows plots of inelastic (plastic in this case), elastic, and total strainrange versus life for the isothermal and BTF tests. The governing equation for the total strainrange versus cyclic life relations is

$$\Delta\epsilon_t = \Delta\epsilon_{el} + \Delta\epsilon_{in} = B(N_f)^b + C(N_f)^c \qquad (1)$$

Equation constants are listed in table IV(a) for each test type and temperature. The isothermal HRSC (PP) data at 538, 760, and 983 °C reported by PWA (ref. 8) have also been analyzed and the equation constants are also included in table IV(a).

Bithermal creep-fatigue.—The BTC-F results generated on this heat of material were from tests of the bithermal CCOP (PC + PP) type. Data are listed in table III(b). A plot of the inelastic, elastic, and total strainrange versus number of cycles to failure is depicted in figure 4(a). Constants from equation (1) are listed in table IV(b). The figure and table contain results only from plots of the raw strainrange versus life data. When the SRP method is used for life prediction, it is necessary to calculate the "pure" inelastic strainrange versus life relationship in accordance with procedures recommended in reference 14.

Thermomechanical fatigue.—Only out-of-phase, TMOP (PC + PP), TMF results were generated for this alloy. Table III(c) contains the raw data. The inelastic, elastic, and total strainranges versus cycles to failure data are shown in figure 4(b) together with linear regression lines. Constants from equation (1) are listed in table IV(c).

Flow behavior.—The flow response characteristics, in terms of the cyclic elastic strainrange versus inelastic strainrange, for the isothermal, bithermal, and thermomechanical exper-

iments (PP, CP, and PC) are shown in figure 5. The fatigue (PP) data are shown in figure 5(a), while the BTC-F and TMF results (PC + PP) are displayed in figure 5(b). Linear regression analysis curves are shown on the log-log plots. The general equation is written as

$$\Delta\epsilon_{el} = K(\Delta\epsilon_{in})^n \tag{2}$$

Equation constants K and n are listed in tables IV(a) to (c). Also listed in table IV are the ratios b/c for comparison with the measured values of n.

Failure mechanisms.—No metallographic or fractographic examination has been made of the failed specimens in the current program. However, for B1900+Hf, Nelson, Schoendorf, and Lin (ref. 8) have ascertained that cracks in their isothermal HRSC (PP) and TMF, TMIP (CP + PP) and TMOP (PC + PP) tests always originated at microscopic casting pores or carbides located at or very near the specimen surface. Cracks propagated in a transgranular mode at isothermal temperatures up to about 871 °C where they propagated in mixed transgranular and intergranular modes. In-phase TMF tests at cyclic temperatures of 871 ↔ 538 °C failed by intergranular crack propagation, and the out-of-phase TMF test specimens failed transgranularly. Since our specimens were prepared from the same heat of material as used by Nelson, Schoendorf, and Lin (ref. 8), we might expect to observe similar crack initiation and propagation mechanisms under similar test conditions.

Haynes 188 Flow and Failure Behavior

Tensile tests.—Tensile test characteristics were not measured on this heat of Haynes 188. Handbook tensile data from reference 9 are reproduced in table II(b) for completeness.

Isothermal and bithermal fatigue.—The only isothermal fatigue data (table III(a)) generated on this heat of material were from HRSC (PP) tests reported in reference 10 at temperatures of 316, 704, 760, and 927 °C. Two sets of BTF data were generated (table III(b)) using the HRIP (inphase, PP) and HROP (out-of-phase, PP) type tests with 316 and 760 °C being the minimum and maximum imposed temperatures. Plots of the inelastic (plastic), elastic, and total strainrange versus number of cycles to failure are depicted in figure 6. Linear regression analysis curves are shown in the log-log plots. Equation (1) constants are listed in table IV(a).

Bithermal creep-fatigue.—Two sets of BTC-F results were generated: inphase TCIP (CP + PP) and out-of-phase TCOP (PC + PP). Raw data from these tests are tabulated in table III(b) and plotted as inelastic, elastic, and total strainrange versus cycles to failure in figures 7(a) and (b). Linear regression analysis curves are shown in the log-log plots. Equation (1) constants are listed in table IV(b).

Thermomechanical fatigue.—Both inphase TMIP (CP + PP) and out-of-phase TMOP (PC + PP) TMF fatigue results were generated for this alloy. Table III(c) contains the raw data which are plotted as inelastic, elastic, and total strainrange versus number of cycles to failure in figures 7(c) and (d). Linear regression analysis curves are shown in the log-log plots. Equation (1) constants are listed in table IV(c).

Flow behavior.—The flow response characteristics of the PP results (isothermal and bithermal, in-phase and out-of-phase) are shown in figure 8(a) as plots of elastic strainrange versus inelastic (plastic in this case) strainrange on log-log coordinates. Similar flow response results for the BTC-F and TMF tests are shown in figure 8(b). Linear regression analysis curves are shown in the log-log plots. Equation (2) constants are listed in table IV.

Failure mechanisms.—No metallographic or fractographic examination has been made of the failed specimens in the current program.

Discussion of Results

The primary purpose for this experimental investigation was to provide a data base for evaluation of the TMF/TS-SRP life prediction method. However, it is worthwhile to examine these results on their own merits, and to point out trends in material behavior.

These trends, as reflected by constants in equations (1) and (2), are masked by the limited number of tests performed under each isothermal, bithermal, or thermomechanical condition. Attempts to summarize the results with linear regression analyses of the data over very limited ranges of life and strainrange occasionally resulted in abnormally low or high values of the exponents b, c, and n. These, in turn, lead to correspondingly low or high values of the coefficients B, C, and K. Although the equations represent the data accurately within their limited range, they can be misleading when extrapolated. Hence, these coefficients alone do not adequately indicate the relative positions of the various sets of data. We have overcome this dilemma by reducing the influence of exponent variations on the equation coefficients. An average value for each exponent has been selected and forced through each set of data. The resultant coefficients give a much better indication of the relative location of one set of data to another. Average exponent values were found to be as follows: $b = -0.13$, $c = -0.70$, and $n = b/c = 0.186$. Thus,

$$\Delta\epsilon_t = B'(N_f)^{-0.13} + C'(N_f)^{-0.70} \tag{3}$$

and

$$\Delta\epsilon_{el} = K'(\Delta\epsilon_{in})^{0.186} \tag{4}$$

Table V lists the values of B', C', and K' for each data set. We are now in a better position to point out data trends by examining variations of the newly defined coefficients.

The first relationship to be explored is that between tensile ductility and cyclic strain resistance. It is reasonable to examine

this possibility since the temperatures for the BTC-F and TMF tests were selected on the basis of the shape of the curve of tensile ductility versus temperature. We shall look first at the isothermal cyclic plastic strain resistance before considering the bithermal and thermomechanical results.

Isothermal HRSC (PP).—The coefficients C', determined from the B1900+Hf HRSC (PP) tests at five isothermal temperatures, form the curve shown in figure 9(a). Superimposed over this curve is the tensile ductility (percent elongation) versus temperature curve from figure 2(a). The minimum in the ductility curve is also observed in the curve of C' versus temperature. Despite the small shift in the temperature at which the minimum occurs, there is excellent qualitative correlation between tensile elongation and isothermal HRSC (PP) fatigue resistance. Just as important a more global observation is that B1900+Hf exhibits a tensile ductility of only one-tenth that of Haynes 188 (i.e., 4 to 7 percent elongation versus 43 to 73 percent), and the corresponding C' values for B1900+Hf are also on the order of one-tenth or less of those for Haynes 188 (0.05 to 0.14 versus 0.5 to 3.3). The Haynes 188 results are plotted in figure 9(b). In this figure, excellent qualitative correlation again is shown. Both the percent elongation and the C' versus temperature curves pass through a significant minimum in the vicinity of 760 °C.

Let us now examine the isothermal HRSC (PP) elastic strainrange versus life relations for the two alloys. Correlation between the cyclic coefficient B' and the monotonic tensile property ultimate tensile strength/elastic modulus (UTS/E) is shown in figures 9(c) and (d), for B1900+Hf and Haynes 188, respectively. Excellent qualitative correlation is shown in these cases. The superior elastic strainrange resistance of the B1900+Hf over the Haynes 188 is clearly shown at all temperature levels. Correlations of the cyclic flow behavior, as indicated by the coefficient K', is also shown in figures 9(c) and (d). Variations of the isothermal values of K' and B' with temperature exhibit similar trends.

Additional observations.—The mechanical behavior trends noted here persist despite the vast differences in obvious rates of oxidation attack over the wide range of temperatures. This leads to the conclusion that the high-temperature fatigue (PP) resistance is governed to a greater extent by the bulk mechanical properties (ductility, strength, and stiffness) than by the highly localized surface and oxidation characteristics. This does not imply a lack of influence of environment, but rather that, under these conditions, any influencing role of the environment appears to be secondary.

Bithermal flow and failure behavior.—Let us now examine the effect of bithermal cycling on the flow and failure response.

The C' intercepts for HROP (PP) out-of-phase bithermal cycling of both B1900+Hf and Haynes 188 are above the isothermally measured HRSC (PP) values at the maximum bithermal temperature. This implies a greater inelastic strain-cycling failure resistance due to thermal cycling than found isothermally. This is a rare and unexpected occurrence (ref. 15). Lack of HRIP inphase bithermal data for B1900+Hf prevents further comparisons of PP results for this alloy. The Haynes 188 behaves in the more conventional manner, and the HRIP (PP) bithermal intercept C' is less than any of the isothermal values.

The HROP and HRIP B' intercept values for the two alloys do not exhibit any distinct trends relative to the isothermal HRSC behavior. This may be because B' is actually a combination of failure (C') and flow (K') behavior (ref. 3). The influences of cycle type and temperature may be consistent for the individual behaviors, but because of their combination, those consistencies may not carry through into B'.

The HROP flow response of the B1900+Hf, as measured by K', is as expected; that is, it is intermediate to that of the isothermal HRSC K' values at the maximum and minimum temperatures of the bithermal cycle. The same is not true for the Haynes 188, wherein the bithermal values are greater than any of the isothermal ones. This latter result implies a greater degree of cyclic strain hardening in the bithermal PP tests than was present isothermally. As one might expect, the HRIP and HROP K' values are nearly identical.

Bithermal creep-fatigue.—The CCOP out-of-phase BTC-F (PC) results for both alloys exhibit lower inelastic (C') and elastic (B') strainrange coefficients than the corresponding out-of-phase bithermal PP results. Thus there appears to be a detrimental effect on life with increased time at temperature during the creep portion of these cycles. The TCIP inphase BTC-F (CP) results for the Haynes 188 show an even further degradation in cyclic strain resistance, much as the HRIP inphase fatigue resistance was below that of the HROP out-of-phase tests. Whether these degradations are due primarily to creep-plasticity interactions, oxidation, or a combination of mechanisms cannot be determined from the data at hand. The flow resistance, as measured by K', exhibited by the BTC-F (CP or PC + PP) tests was also less than that of the BTF (PP) tests. This is conventional behavior and is indicative that negative strain rate hardening mechanisms (such as time-dependent precipitation hardening) probably do not contribute to the complex cyclic strain hardening behavior.

Thermomechanical fatigue.—A direct comparison of the TMF results with the bithermal fatigue and bithermal creep-fatigue results is given in figure 10(a) for the out-of-phase tests on B1900+Hf and in figures 10(b) and (c), respectively, for the out-of-phase and inphase tests on Haynes 188. The TMF/TS-SRP approach (ref. 4) normally considers the bithermal fatigue curves (HRIP and HROP) to represent upper bounds on the expected TMF lives. Correspondingly, lower bounds on expected TMF lives would be derived from the bithermal creep-fatigue curves (TCIP or CCOP). The TCIP and CCOP curves shown in figure 10 are not lower bounds because the inelastic components of strainrange have not been partitioned and hence represent only plots of the raw data. A companion paper (ref. 3) includes the results of analytically partitioning the bithermal creep-fatigue and thermomechanical test results that are necessary for making TMF life predictions. For now, we can only examine the direct comparison of the raw data.

Out-of-phase TMF cycling of the B1900+Hf resulted in life degradation relative to the out-of-phase BTC–F cycling; that is, both intercepts C' and B' decreased. This is contrary to what has been observed for other, more ductile materials (see, for example, ref. 11) and what is found currently for the ductile Haynes 188. The latter behavior is expected on the basis of the concepts of SRP. The BTC–F tests typically contain a greater fraction of creep strain than the TMF tests. There are two reasons for this: (1) considerably more time is usually spent at the highest bithermal temperature, and (2) creep strain is emphasized by holding the stress constant during the creeping portion of the BTC–F cycle. Since cyclic creep strains are typically more damaging than cyclic plasticity, cyclic life suffers in the BTC–F test compared to the TMF test. Analytic partitioning (ref. 3) of the inelastic strains in the TMF cycles indicated that they have a smaller component of PC strains than do the BTC–F tests. The average time per cycle was indeed greater for the bithermal tests.

Greater strain hardening occurred (i.e., larger K') in the TMF tests than in the BTC–F tests. This is expected, since there are greater proportions of creep strains in the BTC–F cycles.

Concluding Remarks

A data base has been generated for the evaluation of the TMF/TS–SRP high-temperature creep-fatigue life prediction method (ref. 3). Bithermal fatigue, bithermal creep-fatigue, and thermomechanical fatigue experiments have been performed on two aerospace structural alloys: cast B1900+Hf and wrought Haynes 188. Comparisons have been made between the results of these tests and isothermal tensile and fatigue tests. Qualitative correlations have been observed between tensile and isothermal fatigue tests, but such correlations were not apparent for the more complex bithermal and thermomechanical fatigue results.

Appendix—Calculation of Axial Strainrange

The following relations between axial ($\Delta\epsilon$) and diametral ($\Delta\epsilon^D$) strainranges were used to convert diametral strainrange to axial strainrange:

$$\Delta\epsilon_t = \Delta\epsilon_{el} + \Delta\epsilon_{in} \tag{A1}$$

$$\Delta\epsilon_{el} = \left(\frac{\sigma}{E}\right)_{tens} + \left(\frac{\sigma}{E}\right)_{comp} \tag{A2}$$

$$\Delta\epsilon_{in} = \frac{(\Delta\epsilon^D)_{in}}{\mu} \tag{A3}$$

where

μ	0.5 (incompressible condition for inelastic Poisson's ratio)
$(\sigma/E)_{tens}$	elastic strain at the temperature of the peak tensile strain
$(\sigma/E)_{comp}$	elastic strain at the temperature of the peak compressive strain
σ	axial stress
E	modulus of elasticity

References

1. Dennis, A.J.; and Cruse, T.A.: Cost Benefits from Improved Hot Section Life Prediction Technology. AIAA Paper 79-1154, 1979.
2. Sokolowski, D.E.: NASA HOST Project Overview. Toward Improved Durability in Advanced Aircraft Engine Hot Sections, D.E. Sokolowski, ed., American Society of Mechanical Engineers, New York, 1988, pp. 1–4.
3. Halford, G.R.; Saltsman, J.F.; Verrilli, M.J., and Arya, V.: Application of a New Thermal Fatigue Life Prediction Model to Two High-Temperature Aerospace Alloys. NASA TM-4226, 1990. (Submitted to the ASTM for inclusion in Advances in Fatigue Lifetime Predictive Techniques, ASTM STP 1122, 1991, M.R. Mitchell and R.W. Landgraf, eds., American Society for Testing and Materials, Philadelphia, PA.)
4. Saltsman, J.F.; and Halford, G.R.: Life Prediction of Thermomechanical Fatigue Using the Total Strain Version of Strainrange Partitioning (SRP)—A Proposal. NASA TP-2779, 1988.
5. Saltsman, J.F.; and Halford, G.R.: Procedures for Characterizing an Alloy and Predicting Cyclic Life With the Total Strain Version of Strainrange Partitioning. NASA TM-4102, 1989.
6. Moreno, V.: Creep Fatigue Life Prediction for Engine Hot Section Materials (Isotropic). NASA CR-168228, 1983.
7. Moreno, V.; Nissley, D.M.; and Lin, L.S.: Creep Fatigue Life Prediction for Engine Hot Section Materials (Isotropic). NASA CR-174844, 1984.
8. Nelson, R.S.; Schoendorf, J.F.; and Lin, L.S.: Creep Fatigue Life Prediction for Engine Hot Section Materials (Isotropic). NASA CR-179550, 1986.
9. Nickel Base Alloys, International Nickel Company, Inc., New York, 1977.
10. Halford, G.R.; Saltsman, J.F.; and Kalluri, S.: High Temperature Fatigue Behavior of Haynes 188. Advanced Earth-to-Orbit Propulsion Technology Conference, NASA CP-3012, Vol. I, R.J. Richmond and S.T. Wu, eds., 1988, pp. 497–509.
11. Halford, G.R., et al.: Bithermal Fatigue—A Link Between Isothermal and Thermomechanical Fatigue. Low Cycle Fatigue, ASTM STP-942, H.D. Solomon, G.R. Halford, L.R. Kaisand, and B.N. Leis, eds., American Society for Testing and Materials, Philadelphia, PA, 1988, pp. 625–637.
12. McGaw, M.A.; and Bartolotta, P.A.: The NASA Lewis Research Center High Temperature Fatigue and Structures Laboratory. Proceedings, 4th Annual Hostile Environments and High Temperature Measurements Conference, Society for Experimental Mechanics, Inc., Bethel, CT, 1987, pp. 12–29.
13. Manson, S.S.; and Halford, G.R.: Re-examination of Cumulative Fatigue Damage Analysis—An Engineering Perspective. Eng. Fract. Mech., vol. 25, no. 5/6, 1986, pp. 539–571.
14. Hirschberg, M.H.; and Halford, G.R.: Use of Strainrange Partitioning to Predict High-Temperature Low-Cycle Fatigue Life. NASA TN D-8072, 1976.
15. Halford, G.R.: Low-Cycle Thermal Fatigue. Thermal Stresses II, R.B. Hetnarski, ed., Elsevier Science Publishers, Amsterdam, 1987, pp. 329–428.

TABLE I.—TYPES AND CONDITIONS OF FATIGUE TESTS CONDUCTED

Fatigue test type	Test temperature, °C	
	B1900+Hf	Haynes 188
Isothermal HRSC (PP)	483	316
	[a]538	---
	[a]760	704
	871	760
	[a]983	927
Bithermal		
HRIP (PP)	------	760 – 316
HROP (PP)	[b]483 – 871	316 – 760
TCIP (CP + PP)	------	760 – 316
CCOP (PC + PP)	483 – 871	316 – 760
Thermomechanical		
TMIP inphase (CP + PP)	------	760 – 316
TMOP out-of-phase (PC + PP)	483 – 871	316 – 760

[a]Isothermal fatigue (HRSC) data at 0.083 to 0.17 Hz have been reported in reference 8 on the same heat of alloy; raw data not repeated herein.
[b]The symbol – denotes thermal cycling; the first value is extreme temperature in tension; the second is extreme temperature in compression.

TABLE II.—TENSILE PROPERTIES

Temperature, °C	Elastic modulus, *E*, GPa	Yield strength, YS, MPa	Ultimate tensile strength, UTS, MPa	UTS/*E*	Tensile elongation,[b] percent
B1900+Hf					
260	[a]170	[a]702	[a]888	0.0052	---
483	[a,c]154	---	---	------	---
538	[a]150	[a]727	---	-----	7.0
760	[a]141	[a]727	[a]899	.0064	4.0
871	[a]146	[a]617	[a]786	.0054	4.0
982	[a]126	[a]322	[a]478	.0038	7.0
Haynes 188[b]					
316	[c]204	---	---	-----	---
538	[c]192	305	740	0.0039	70.0
649	185	305	710	.0038	61.0
704	[c]181	---	---	-----	---
760	[c]175	290	635	.0036	43.0
871	166	260	420	.0025	73.0
927	[c]160	---	---	-----	---
982	[c]155	162	255	.0016	72.0

[a]Averages of values reported in reference 7.
[b]Handbook values from reference 9.
[c]Interpolated value.

TABLE III.—ISOTHERMAL FATIGUE, BITHERMAL FATIGUE AND CREEP-FATIGUE, AND THERMOMECHANICAL FATIGUE RESULTS

(a) Isothermal fatigue, HRSC (PP) tests

Test temperature, °C	Test frequency, Hz	Strainranges, percent			Stress range, MPa	Cycles to failure, N_f
		Elastic	Inelastic	Total		
B1900+Hf						
[a]483	0.2	1.10	0.48	1.58	2085	33
	.2	.91	.08	.99	1717	742
	.2	.80	.02	.82	1527	3 094
[a]871	0.2	0.88	0.31	1.19	1254	139
	.2	.87	.21	1.08	1234	214
	.2	.43	.01	.44	616	17 731
Haynes 188						
316	0.2	0.62	2.55	3.17	1276	995
	.2	.55	1.05	1.60	1118	4 959
	.2	.47	.35	.82	967	17 678
704	0.2	0.79	1.58	2.37	1425	281
	.5	.69	.94	1.63	1248	524
	↓	.67	.83	1.50	1208	652
		.66	.84	1.50	1187	885
		.67	.87	1.54	1215	954
		.63	.53	1.16	1134	1 477
		.49	.30	.79	889	3 797
		.43	.19	.62	780	15 705
		.42	.06	.48	759	21 399
		.45	.11	.56	818	22 125
		.46	.04	.50	836	51 438
760	0.4	0.96	8.90	9.86	1672	13
	↓	.64	.90	1.54	1121	302
		.59	.68	1 27	1037	400
		.62	.63	1.25	1086	445
		.67	.26	.93	1180	709
		.62	.41	1.03	1084	1 370
		.59	.21	.80	1026	1 977
		.50	.31	.81	877	2 142
	29.0	.48	.14	.62	835	4 500
	.4	.47	.10	.57	819	4 918
	29.0	.46	.10	.56	807	7 900
	29.0	.42	.11	.53	742	11 300
927	0.2	0.40	1.79	2.19	645	295
	↓	.42	1.80	2.22	666	372
		.38	.74	1.12	605	921
		.36	.78	1.14	568	1 985
		.31	.14	.45	496	10 885
		.30	.16	.46	488	12 568

[a]Strainrange values differ slightly from reference 11 due to differences in values of elastic moduli. Current values were determined from measured moduli for this heat of B1900+Hf (ref. 7).

TABLE III.—Concluded.

(b) Bithermal fatigue (PP) and bithermal creep-fatigue (CP or PC + PP) tests

Test type	Test temperature, °C	Strainranges, percent			Stress at peak tensile strain, σ_{tens}, MPa	Stress at peak compressive strain, σ_{comp}, MPa	Stress range, $(\sigma_{tens} - \sigma_{comp})$, MPa	Failure life	
		Elastic	Inelastic	Total				Cycles to failure, N_f	Time to failure,[b] t_f, hr
B1900+Hf									
HROP	483–871	1.11	0.59	1.70	853	−912	1765	142	----
		1.06	.27	1.33	824	−870	1694	234	13.6
		.72	.07	.79	651	−520	1171	880	----
CCOP	483–871	1.10	0.84	1.94	955	−695	1650	44	1.3
		.83	.66	1.49	793	−560	1353	96	10.1
		.95	.30	1.25	971	−753	1724	179	89.7
		.90	.32	1.22	729	−712	1441	220	28.3
Haynes 188									
HRIP	760–316	0.91	2.73	3.64	798	−929	1727	40	2.5
		.70	.67	1.37	628	−691	1319	350	21.0
		.60	.35	.95	541	−598	1139	1421	78.9
HROP	316–760	0.86	1.67	2.53	823	−796	1619	213	12.0
		.81	1.30	2.11	806	−734	1540	304	18.5
		.74	.69	1.43	737	−660	1397	682	47.4
		.71	.56	1.27	692	−692	1335	955	56.7
		.63	.34	.97	620	−570	1190	2799	163.2
TCIP	760–316	0.56	1.27	1.83	368	−712	1080	59	83.8
		.53	.55	1.08	353	−673	1026	375	63.9
		.50	.21	.71	379	−583	962	1940	137.8
CCOP	316–760	0.59	2.66	3.25	815	−333	1148	52	62.1
		.55	1.05	1.60	736	−332	1068	215	266.0
		.50	.56	1.06	664	−299	963	647	133.9

(c) Thermomechanical fatigue tests

B1900+Hf[c]									
TMOP	483–871	1.55	1.67	3.22	1563	−989	2552	16	1.1
		.94	.53	1.47	942	−599	1541	55	3.7
		.91	.47	1.38	916	−577	1493	67	4.5
		.85	.20	1.05	839	−557	1396	124	8.3
		.65	.07	.72	728	−365	1093	546	36.4
		.46	.01	.47	628	−170	798	1992	132.8
Haynes 188[c]									
TMIP	760–316	0.84	2.67	3.51	725	−874	1599	28	1.4
		.83	2.07	2.90	712	−855	1567	39	2.0
		.70	.46	1.16	543	−794	1337	829	41.1
TMOP	316–760	0.84	1.62	2.46	912	−691	1603	191	9.6
		.73	.63	1.36	872	−542	1414	477	23.9
		.56	.27	.83	661	−415	1076	720	36.0

[b]Includes time at zero load during temperature changes between maximum and minimum during bithermal cycling.

[c]Thermomechanical cycle times were 4 and 3 min/cycle for the B1900+Hf and the Haynes 188, respectively.

TABLE IV.—CONSTANTS FOR FLOW AND FAILURE BEHAVIOR
[Least squares curve fit of log-log data plots.]

(a) Isothermal and Bithermal Fatigue (PP)

Test type	Temperature, °C	Coefficients			Exponents			
		C	B	K	c	b	n	b/c
B1900+Hf[a]								
HRSC	483	0.071	0.014	0.018	−0.73	−0.07	0.094	0.093
	538	.089	.025	.025	−.89	−.17	.15	.20
	760	.012	.033	.101	−.63	−.21	.30	.34
	871	.067	.019	.036	−.63	−.15	.24	.24
	982	.099	.017	.022	−.63	−.21	.25	.34
HROP	483–871	1.96	.041	.033	−1.19	− .26	.20	.22
Haynes 188								
HRSC	316	3.39	0.012	0.010	−0.70	−0.096	0.14	0.14
	704	.83	.016	.015	−.69	−.13	.17	.19
	760	.50	.014	.014	−.70	−.13	.16	.18
	927	1.13	.0066	.0065	−.70	−.081	.11	.12
HRIP	760–316	.23	.014	.019	−.59	−.12	.20	.20
HROP	316–760	.49	.016	.019	−.64	−.12	.19	.19

(b) Bithermal creep-fatigue (CP or PC + PP)

B1900+Hf								
CCOP	483–871	0.176	0.015	0.019	−0.76	−0.096	0.13	0.13
Haynes 188								
TCIP	760–316	0.11	0.0064	0.0073	−0.51	−0.032	0.061	0.061
CCOP	316–760	.30	.0078	.0088	−.62	−.070	.11	.11

(c) Thermomechanical fatigue (CP or PC + PP)

B1900+Hf								
TMOP	483–871	0.33	0.027	0.033	−1.03	−0.24	0.22	0.23
Haynes 188								
TMIP	760–316	0.14	0.010	0.012	−0.51	−0.055	0.11	0.11
TMOP	316–760	19.4	.052	.022	−1.33	−.33	.23	.25

[a]HRSC results at 538, 760, and 982 °C are based on PWA (ref. 8) data.

TABLE V.—COEFFICIENTS C', B', AND K' BASED ON EQUATIONS (3) AND (4)
[$b = -0.13$, $c = -0.70$, and $n = b/c = 0.186$.]

Test type	Temperature, °C	C'	B'	K'
B1900+Hf[a]				
HRSC	483	0.0553	0.0193	0.0327
HRSC	538	.0889	.0247	.0345
HRSC	760	.0124	.0326	.0365
HRSC	871	.0963	.0168	.0258
HRSC	983	.143	.0103	.0144
HROP	483 ↔ 871	.1633	.0203	.0297
CCOP	483 ↔ 871	.1290	.0174	.0253
TMOP	483 ↔ 871	.1075	.0171	.0277
Haynes 188				
HRSC	316	3.277	0.0161	0.0128
HRSC	704	.837	.0160	.0163
HRSC	760	.534	.0141	.0154
HRSC	927	1.035	.0092	.0091
HRIP	760 ↔ 316	.364	.0149	.0176
HROP	316 ↔ 760	.706	.0173	.0178
TCIP	760 ↔ 316	.231	.0109	.0138
CCOP	316 ↔ 760	.429	.0106	.0123
TMIP	760 ↔ 316	.274	.0138	.0172
TMOP	316 ↔ 760	.568	.0156	.0181

[a]HRSC results at 538, 760, and 982 °C are based on PWA (ref. 8) data.

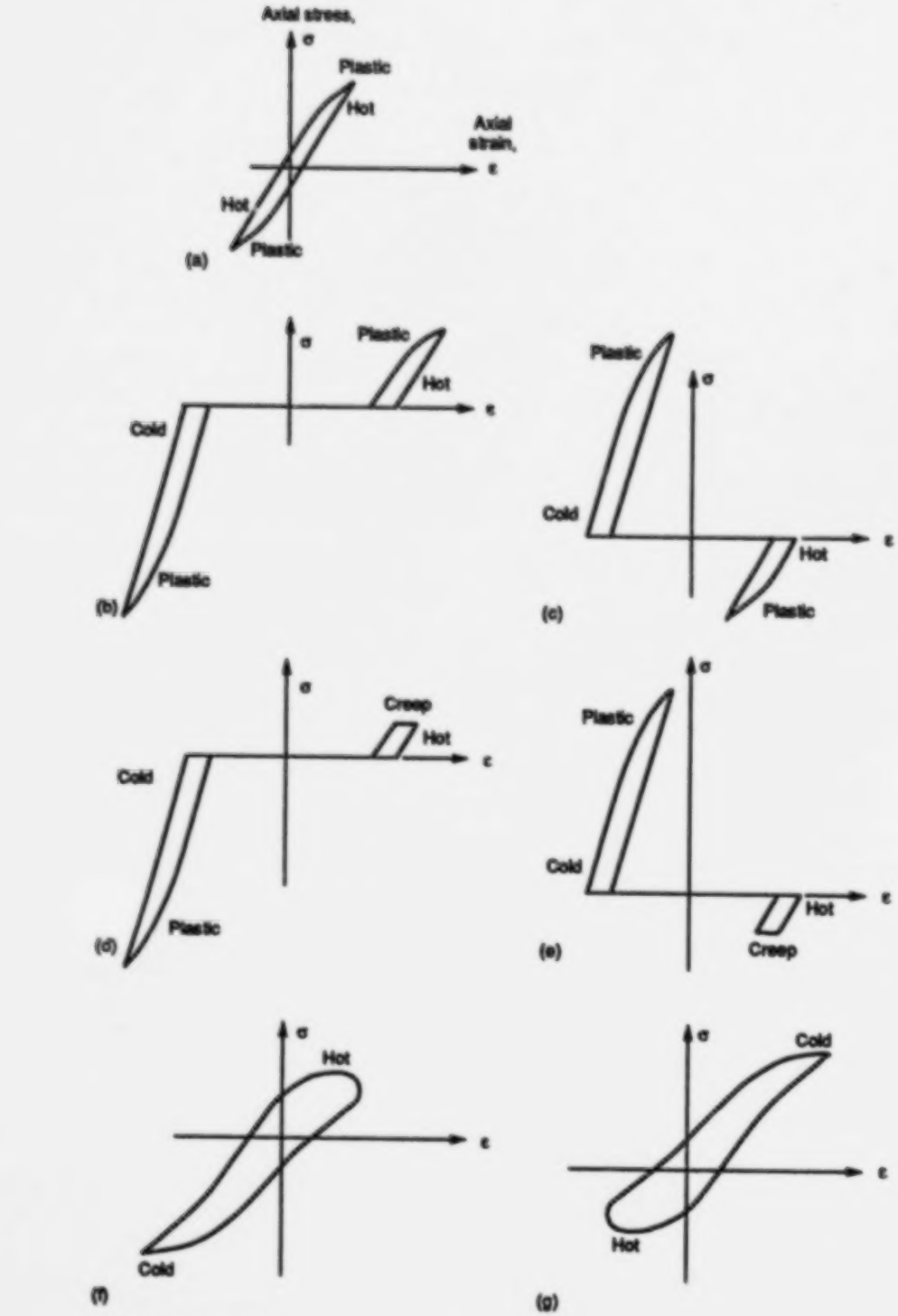

(a) Isothermal HRSC (PP).
(b) Bithermal, inphase HRIP (PP).
(c) Bithermal, out-of-phase HROP (PP).
(d) Bithermal, inphase TCIP (CP + PP).
(e) Bithermal, out-of-phase CCOP (PC + PP).
(f) Thermomechanical, inphase TMIP (CP + PP).
(g) Thermomechanical, out-of-phase TMOP (PC + PP).

Figure 1.—Schematic stress-strain hysteresis loops.

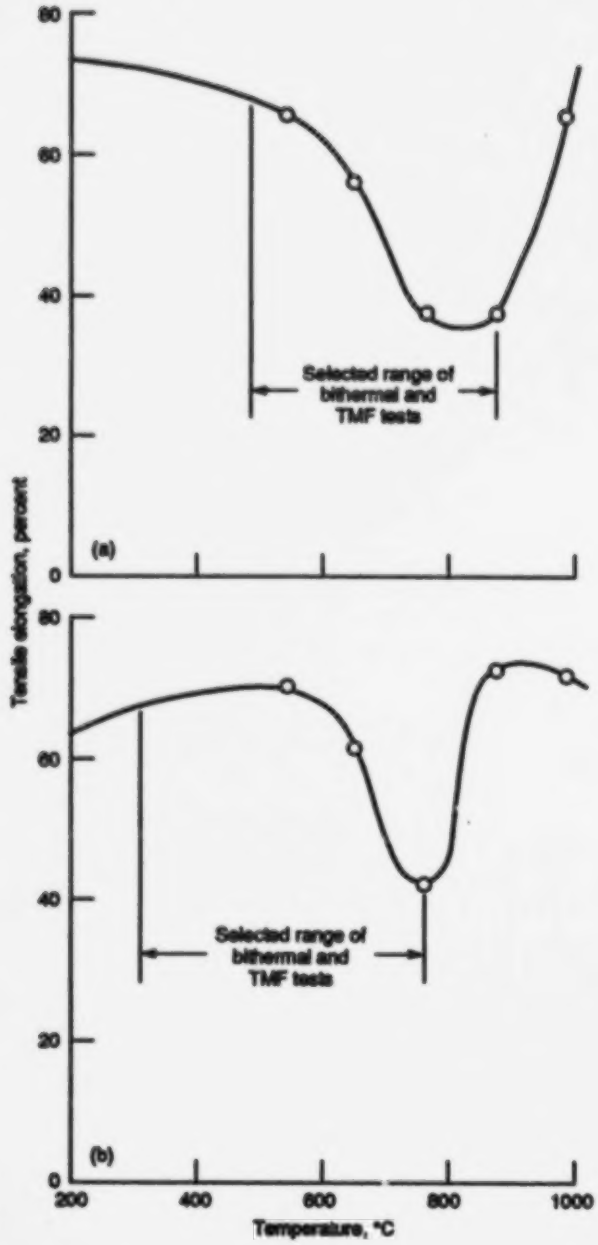

(a) B1900+Hf.
(b) Haynes 188.

Figure 2.—Variation of tensile elongation with test temperature (ref. 9).

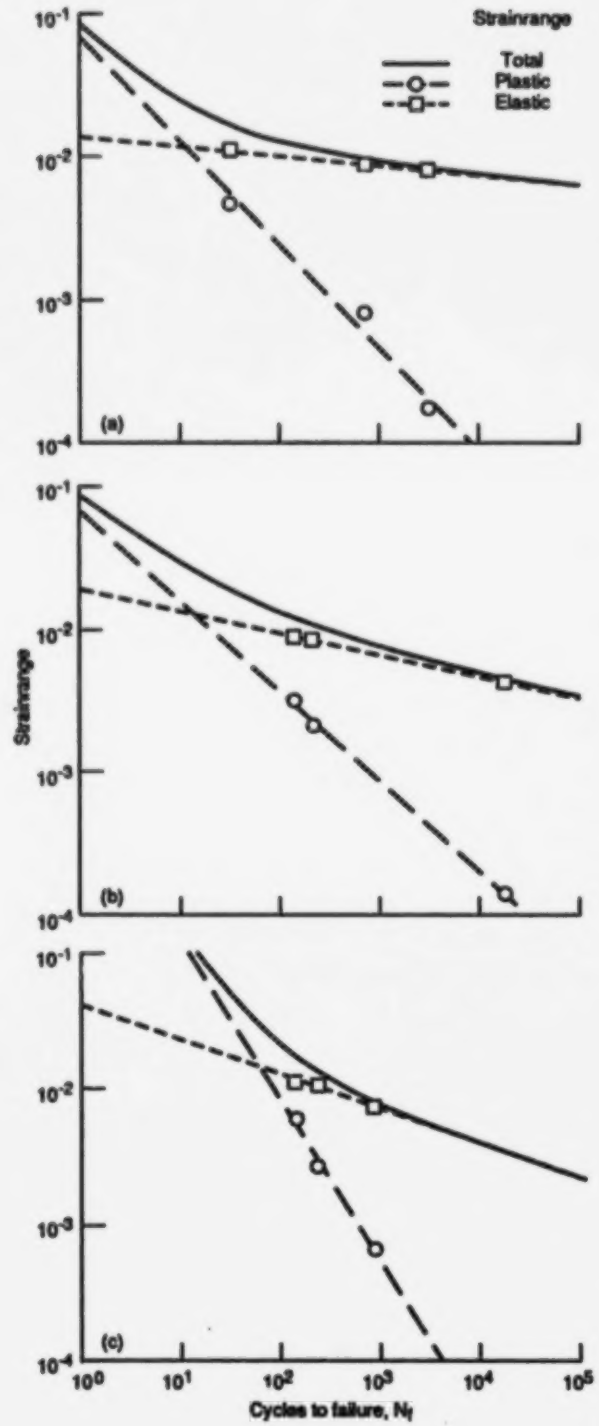

(a) HRSC (PP), 483 °C.
(b) HRSC (PP), 871 °C.
(c) HROP (PP), 483↔871 °C.

Figure 3.—Isothermal HRSC (PP) and bithermal HROP (PP) fatigue failure behavior of B1900+Hf.

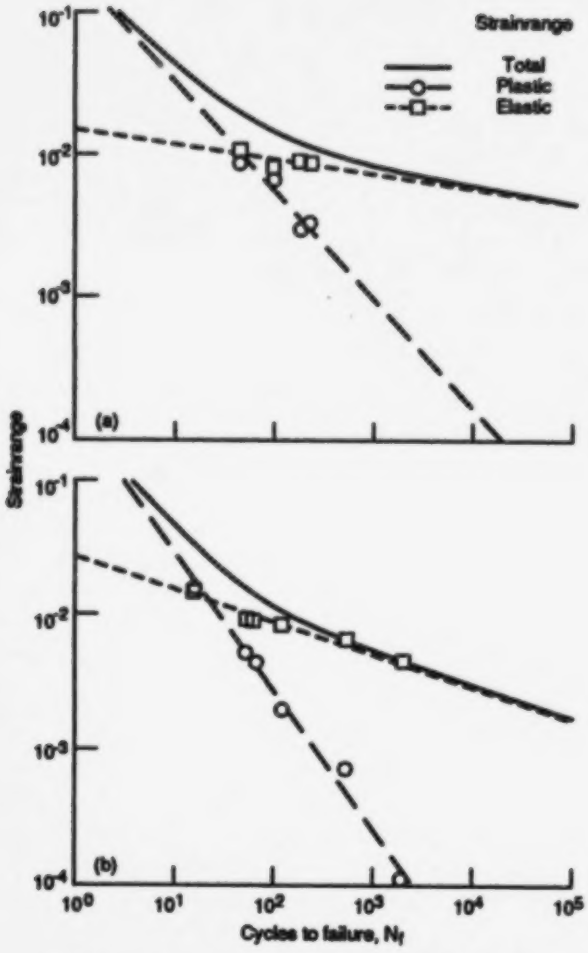

(a) Bithermal, out-of-phase CCOP (PC + PP), 483–871 °C.
(b) Thermomechanical, out-of-phase TMOP (PC + PP), 483–871 °C.

Figure 4.—Bithermal creep-fatigue and thermomechanical fatigue failure behavior of B1900+Hf.

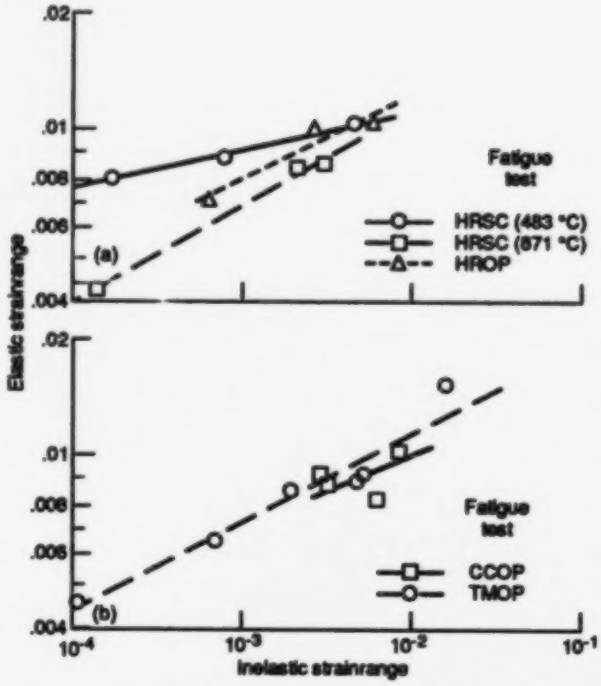

(a) Isothermal and bithermal fatigue (PP).
(b) Bithermal creep-fatigue and thermomechanical fatigue (CP or PC +).

Figure 5.—Cyclic Flow Behavior of B1900+Hf.

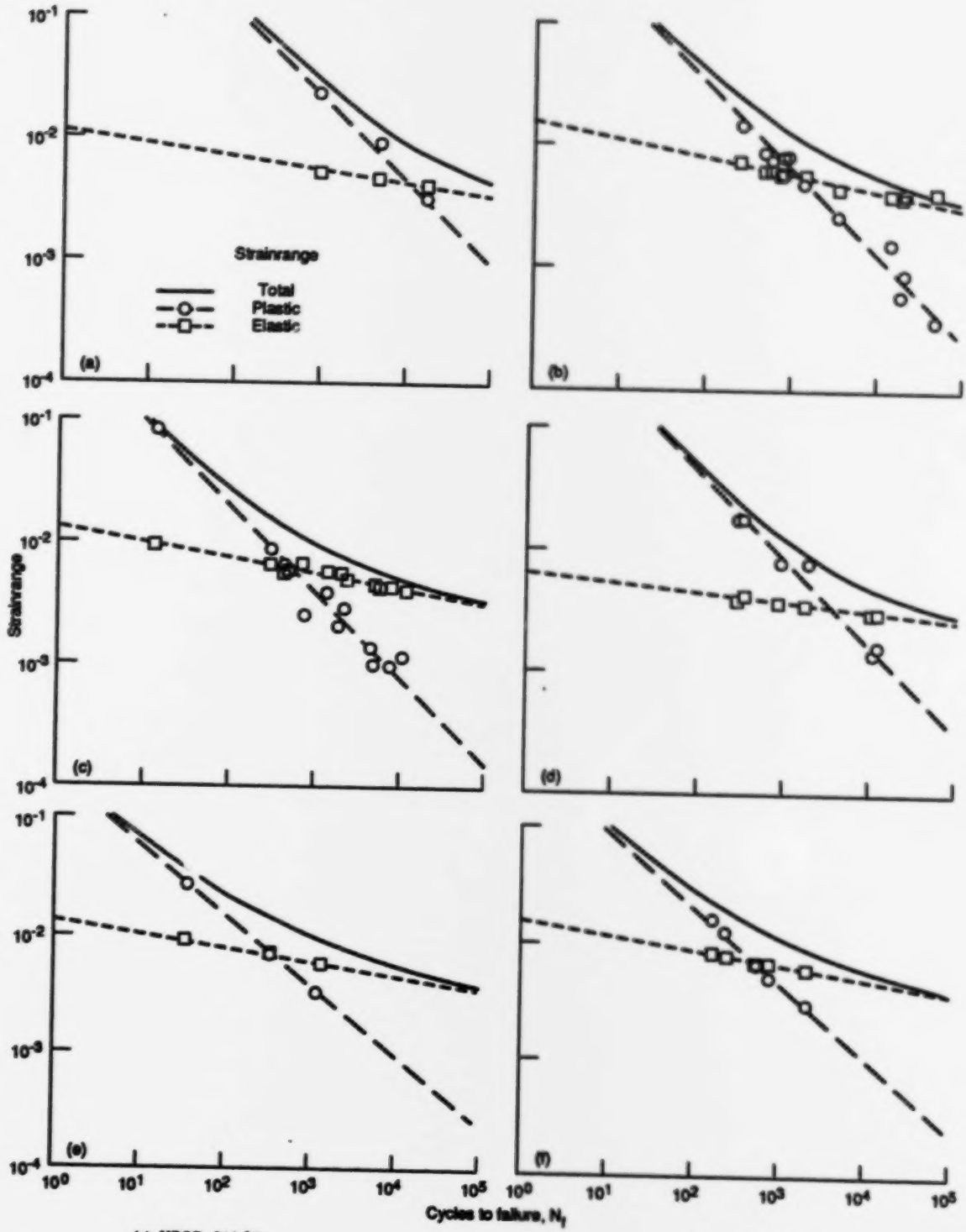

(a) HRSC, 316 °C.
(b) HRSC, 704 °C.
(c) HRSC, 760 °C.
(d) HRSC, 927 °C.
(e) HRIP, 760–316 °C.
(f) HROP, 316–760 °C.

Figure 6.—Isothermal and bithermal fatigue (PP) failure behavior of Haynes 188.

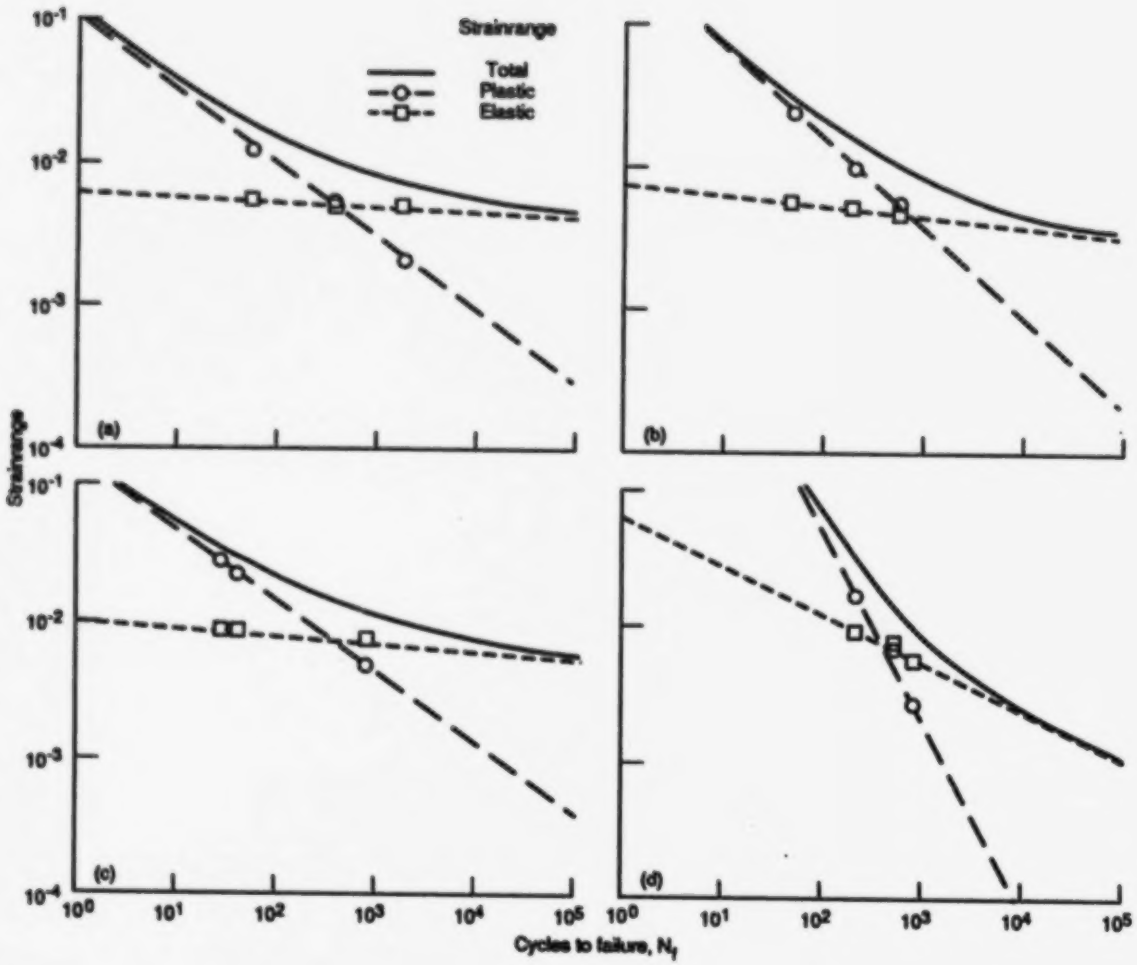

(a) TCIP (CP + PP), 760↔316 °C.
(b) CCOP (PC + PP), 316↔760 °C.
(c) TMIP (CP + PP), 760↔316 °C.
(d) TMOP (PC + PP), 316↔760 °C.

Figure 7.—Bithermal creep-fatigue and thermomechanical fatigue (CP or PC + PP) failure behavior of Haynes 188.

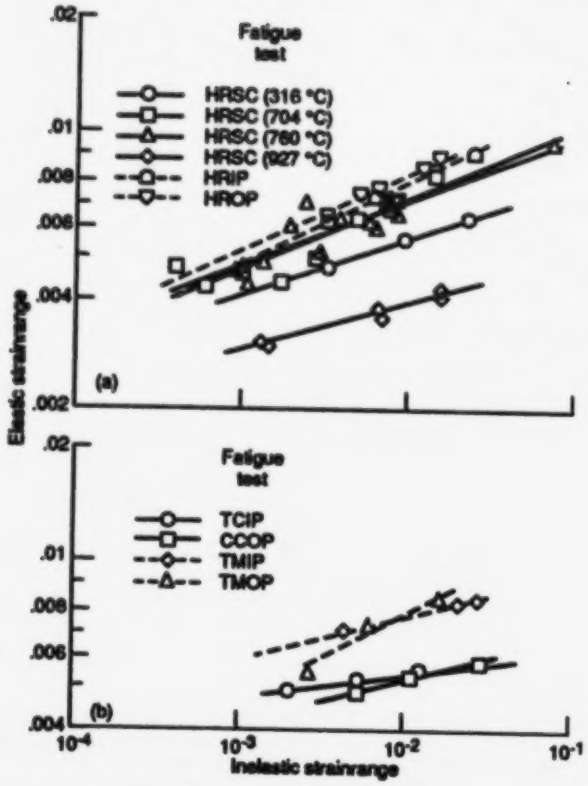

(a) Isothermal and bithermal fatigue (PP).
(b) Bithermal creep-fatigue and thermomechanical fatigue (CP or PC + PP).

Figure 8.—Cyclic flow behavior of Haynes 188.

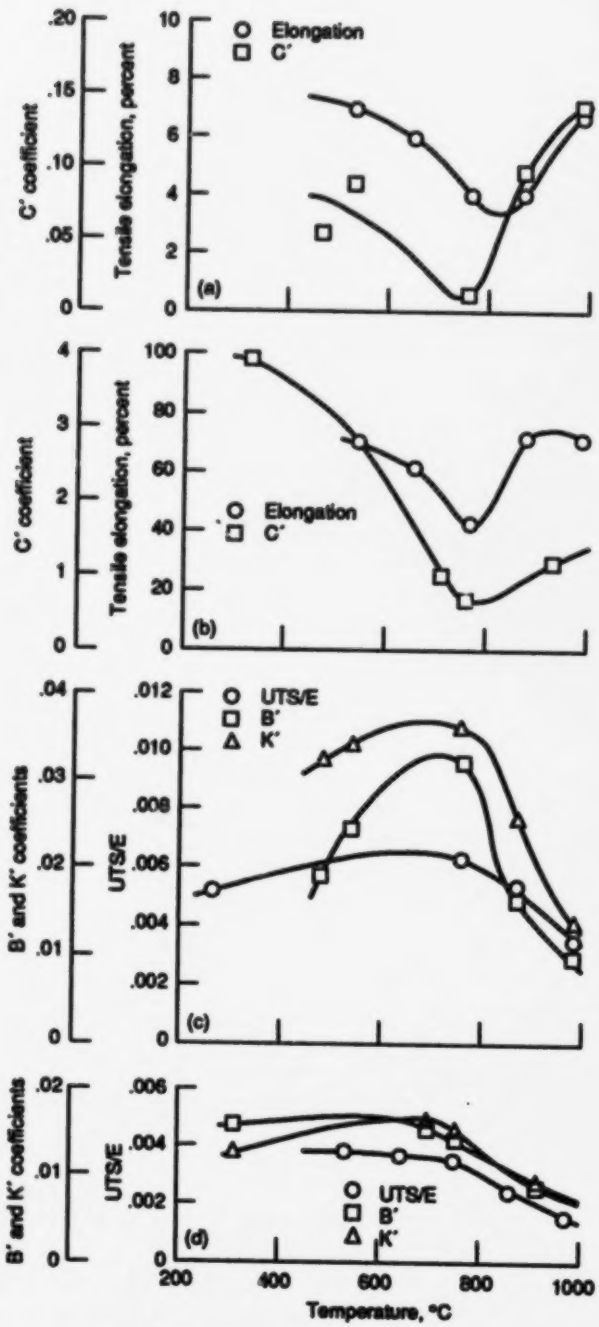

(a) B1900+Hf ductility and C′ coefficient.
(b) Haynes 188 ductility and C′ coefficient.
(c) B1900+Hf UTS/E and B′ and K′ coefficients.
(d) Haynes 188 UTS/E and B′ and K′ coefficients.

Figure 9.—Correlation of tensile properties with isothermal fatigue flow and failure behavior.

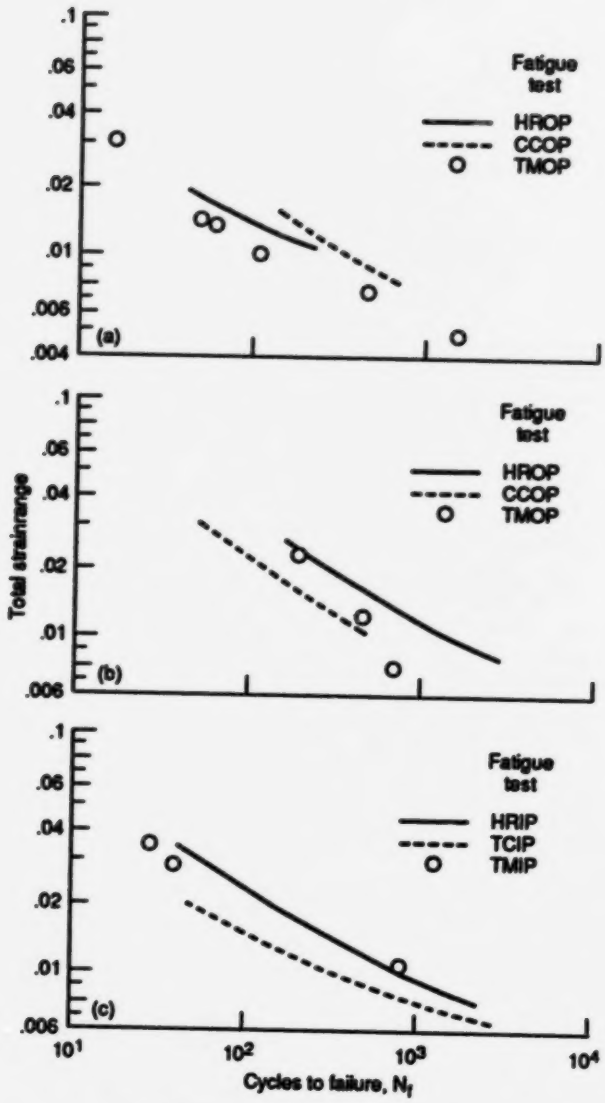

(a) B1900+Hf out-of-phase TMF behavior.
(b) Haynes 188 out-of-phase TMF behavior.
(c) Haynes 188 in-phase TMF behavior.

Figure 10.—Comparison of TMF behavior with bithermal fatigue and bithermal creep-fatigue behavior.

NASA
National Aeronautics and Space Administration

Report Documentation Page

1. Report No.	2. Government Accession No.	3. Recipient's Catalog No.
NASA TM-4225		

4. Title and Subtitle

Thermomechanical and Bithermal Fatigue Behavior of Cast B1900+Hf and Wrought Haynes 188

5. Report Date

April 1991

6. Performing Organization Code

7. Author(s)

Gary R. Halford, Michael J. Verrilli, Sreeramesh Kalluri, Frank J. Ritzert, Rob E. Duckert, and Frederic A. Holland

8. Performing Organization Report No.

E-5601

10. Work Unit No.

553-13-00

9. Performing Organization Name and Address

National Aeronautics and Space Administration
Lewis Research Center
Cleveland, Ohio 44135-3191

11. Contract or Grant No.

13. Type of Report and Period Covered

Technical Memorandum

12. Sponsoring Agency Name and Address

National Aeronautics and Space Administration
Washington, D.C. 20546-0001

14. Sponsoring Agency Code

15. Supplementary Notes

Gary R. Halford, Michael J. Verrilli, Frank J. Ritzert, and Frederic A. Holland, NASA Lewis Research Center. Sreeramesh Kalluri, Sverdrup Technology, Inc., Lewis Research Center Group, 2001 Aerospace Parkway, Brook Park, Ohio 44142. Rob E. Duckert, University of Wisconsin, Dept. of Engineering Mechanics, Madison Wisconsin 53706; presently employed by McDonnell Douglas Corp., St. Louis, Missouri 63166.

16. Abstract

High-temperature thermomechanical and bithermal fatigue behavior was investigated for two superalloys: cast nickel-base B1900+Hf and wrought cobalt-base Haynes 188. Experimental results were generated to support development of an advanced thermal fatigue life prediction method. Strain-controlled thermomechanical and load-controlled, strain-limited, bithermal fatigue tests were used to determine the fatigue crack initiation and cyclic stress-strain response characteristics of the superalloys. Bithermal temperatures of 483 and 871 °C were used for B1900+Hf, and 316 and 760 °C for Haynes 188. Thermomechanical fatigue tests were conducted by using maximum and minimum temperatures corresponding to those for the bithermal experiments. Lives cover the range from about 10 to 3000 cycles to failure. Isothermal fatigue results obtained previously are also discussed.

17. Key Words (Suggested by Author(s))	18. Distribution Statement
Fatigue (metal); Thermomechanical fatigue; Bithermal fatigue; Creep-fatigue; Low-cycle fatigue; High-temperature fatigue; Flow behavior; Failure behavior; Inelastic strain; Strainrange partitioning; Superalloys	Unclassified – Unlimited Subject Categories 26 and 39

19. Security Classif. (of this report)	20. Security Classif. (of this page)	21. No. of pages	22. Price*
Unclassified	Unclassified	23	A03

NASA FORM 1626 OCT 86

*For sale by the National Technical Information Service, Springfield, Virginia 22161

NASA-Langley, 1991

20